Journal of Alloys and Compounds 500 (2010) 56–60

Contents lists available at ScienceDirect

Journal of Alloys and Compounds

journal homepage: www.elsevier.com/locate/jallcom

Effect of phase structure on the dynamic hysteresis scaling behavior in $(1-x)BiScO_3$–$xPbTiO_3$ bulk ceramics

Gang Yu, Xianlin Dong*, Genshui Wang, Fei Cao, Xuefeng Chen

Key laboratory of Inorganic Functional Materials and Devices, Shanghai Institute of Ceramics, Chinese Academy of Sciences, 1295 Dingxi Road, Shanghai 200050, People's Republic of China

ARTICLE INFO

Article history:
Received 19 January 2010
Received in revised form 8 March 2010
Accepted 24 March 2010
Available online 1 April 2010

PACS:
77.80.bj
77.84Dj
77.80Fm

Keywords:
Ferroelectrics
Domain switching
Dynamic hysteresis

ABSTRACT

The ferroelectric hysteresis loops of $(1-x)BiScO_3$–$xPbTiO_3$ (BSPT) ceramics with different phase structure were measured under sinusoidal electric fields. Three-stage behaviors between $\ln\langle A\rangle$ ($\langle A\rangle$ is hysteresis loop area) and $\ln E_0$ (E_0 is the amplitude of field) were identified with the increasing of E_0. These three-stage behaviors reflected different polarization behavior in each stage, which were distinct from the existing two-stage behavior. The shifting of dividing points between two stages with the evolution of phase structure revealed that in the tetragonal phase domain switching has a higher activation field due to the different domain structure.

1. Introduction

$(1-x)BiScO_3$–$xPbTiO_3$ (BSPT) ceramics have drawn more and more attentions due to their comparable piezoelectric properties and considerably high-Curie temperature compared to conventional ceramics such as lead ziconate titanate ceramics [1,2]. For the view point of high-temperature device design, the excellent thermal stability of this kind of material is the basic requirement. Many researchers had pointed out that the thermal stability related to domain state and domain wall motion [2,3]. Thus, a deep understanding of domain dynamics in the tough environment is very essential and urgent for the technical interest. One of the essential problems in domain dynamics is the dynamic of domain switching, i.e. the response of domain switching under sinusoidal external electric fields [4]. Normally, the domain dynamic can be uncovered by the scaling power law, $\langle A\rangle \propto f^{\alpha}E_0^{\beta}$ (where $\langle A\rangle$ is the ferroelectric hysteresis loop area, E_0 is field amplitude, f is frequency, and α, β are exponents), because $\langle A\rangle$ scales the energy dissipation with one period of domain reversal [4]. However, it is complicated to explore the relations between $\langle A\rangle$ and E_0, f in the high-temperature region. Thus, it is necessary to investigate the room temperature (T = 298 K) behavior between $\langle A\rangle$ and f, E_0 first, which can guide our research in the high-temperature region.

Previous investigations have reported the scaling relations in thin films [5,6], soft PZT, hard PZT and $95PbZrO_3$–$5PbTiO_3$ (PZT95/5) bulk ceramics [7–9], and $BaTiO_3$ single crystals [10]. The scaling behavior of dynamic hysteresis revealed that the relation between $\langle A\rangle$ and E_0, f was different in two different field stages (low-E_0 and high-E_0) [7,8,10]. While Viehland had pointed out that polarization reversal behaviors were different in three different stages of external electric field, e.g. $E < E_c$, $E \approx E_c$ and $E > E_c$ (E_c is coercive field) [11,12]. This may suggest that there may be three different scaling relations between $\langle A\rangle$ and E_0, f. Furthermore, the former studies on domain dynamics in hard and soft PZT ceramics revealed that the doping type did not affect the domain dynamic and pointed out that the domain dynamics were mainly dominated by the domain states and structures [7,8]. It is known that the domain structures are different in different phase structures [13]. Thus the domain dynamics in different phase structures should be different. It will be of interest to investigate the domain dynamics in different phase structure, as the direct comparison will help extracting the roles of domain structure to the dynamic hysteresis behavior. Therefore, in this paper we present the results on the scaling behavior of dynamic hysteresis in different field stages and the dynamic hysteresis behaviors in different phase structures. The results shed new light on understanding the evolution of domain switching behavior as the phase structure varied from rhombohedral phase to tetragonal phase.

* Corresponding author.
E-mail address: xldong@sunm.shcnc.ac.cn (X. Dong).

0925-8388/$ – see front matter © 2010 Elsevier B.V. All rights reserved.
doi:10.1016/j.jallcom.2010.03.194

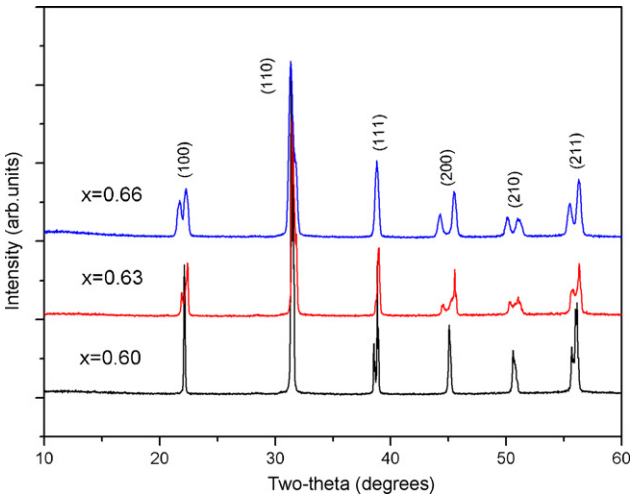

Fig. 1. X-ray diffraction pattern of $(1-x)BiScO_3$–$xPbTiO_3$ ($x = 0.60$, 0.63, 0.66) ceramics (color online).

2. Experimental procedure

BSPT ($x = 0.60$, 0.63, 0.66) ceramics in this study were prepared by the solid-state reaction method. The raw materials were Bi_2O_3 (99.9%), TiO_2 (99.38%), Sc_2O_3 (99.38%), and Pb_3O_4 (99.74%). Aqueous suspensions of raw materials were ball milled for 6 h, and dried at 100 °C. The dried powders were calcined at 700–800 °C for 6 h, and then ball milled again for 24 h to crush the agglomerates. After drying, 6 wt% PVA was mixed into the powders. The mixture was dried, and crushed to pass through a 40-mesh sieve. The powders were then pressed into disks. Following an 800 °C binder burnout, pellets were then sintered in sealed crucibles at 1080–1150 °C for 90 min. All the samples reach a relative high density, which is larger than 96% [2,14]. The dimensions of the samples were Φ5 mm × 0.5 mm. X-ray diffraction (XRD) was performed using an automated diffractometer (Model Rigaku RAX-10 D/max 2550 V, Rigaku Co., Tokyo, Japan) with Cu-$K\alpha_1$ radiation operated at room temperature to determine phase structure and purity within detection limits. The *P*–*E* hysteresis loops of the unpoled samples were measured by aixACCT TF Analyzer 2000 (aixACCT Co., Germany) with high-voltage power supply (TReK Model 663A) at the room temperature (298 K). The hysteresis loop area $\langle A\rangle$ can be calculated by integrating the area bound by the hysteresis loop using the data collection software.

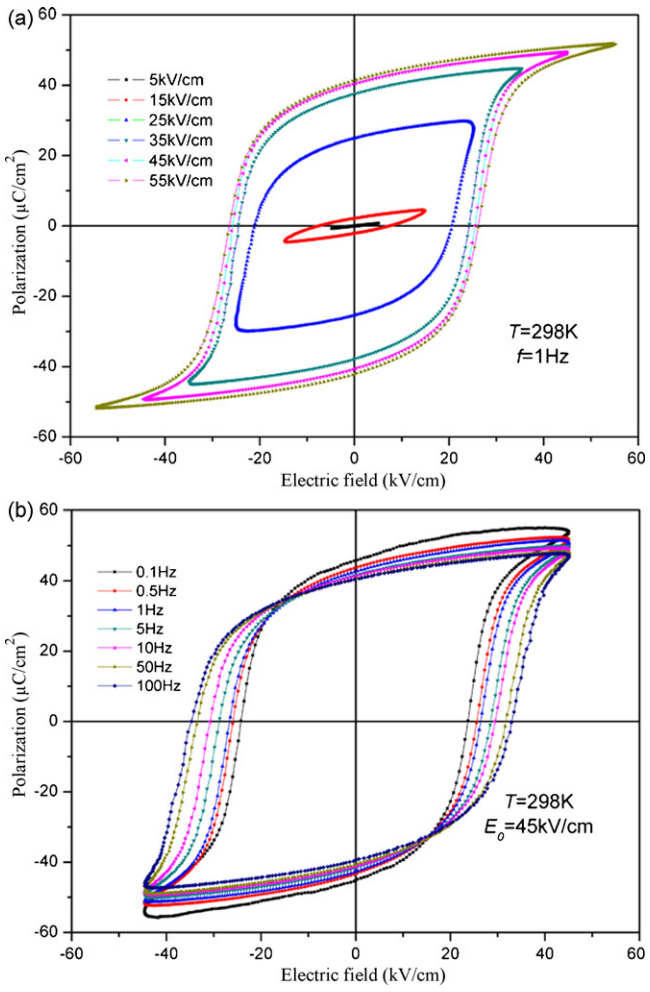

Fig. 2. Hysteresis loops for BSPT37/63 bulk ceramics (a) under different E_0 but fixed $f = 1$ Hz. (b) Under different f but fixed $E_0 = 45$ kV/cm (color online).

3. Results and discussions

Compositions in the $(1-x)BiScO_3$–$xPbTiO_3$ system are characterized with XRD. As presented in Fig. 1, a typical rhombohedral (R) symmetry is observed at room temperature while $x = 0.60$. The presence of morphotropic phase boundary (MPB) is indicated from XRD patterns when $x = 0.63$. The tetragonal (*T*) phase is observed while $x = 0.66$. The lower symmetry phases, being either rhombohedral or tetragonal, are identified by splitting of pseudocubic perovskite peaks $\{h\,k\,l\}$, either $\{1\,1\,1\}$ splitting for rhombohedral, or $\{1\,1\,0\}$ and $\{1\,0\,0\}$ splitting for tetragonal symmetry [14]. In Fig. 2, the hysteresis loops of unpoled $37BiScO_3$–$63PbTiO_3$ (BSPT37/63) ceramics at different E_0 and f are given as an example. As expected, the dependence of the loop profile and area $\langle A\rangle$ on E_0 is remarkable. The hysteresis loops area $\langle A\rangle$, remnant polarization P_r and coercive field E_c increase with the increasing of E_0. But the frequency dependence of hysteresis area $\langle A\rangle$ is ambiguous. Similarly, the hysteresis loops of BSPT40/60 and BSPT34/66 show the similar profile under different E_0 and f. In Fig. 3, the hysteresis loops of BSPT40/60, BSPT37/63 and BSPT34/66 are plotted. It is evident that P_r decreases but E_c increases as the phase structure evolves from rhombohedral phase to tetragonal phase.

In order to investigate the dynamic hysteresis scaling behavior, we plot $\ln\langle A\rangle$ against $\ln E_0$ under different frequency from 0.1 to 100 Hz in three phase structures. Meanwhile, we plot $\mathrm{d}\ln\langle A\rangle/\mathrm{d}\ln E_0$ against $\ln E_0$ in order to guide our data fitting. In Fig. 4, the curves of $\ln\langle A\rangle$ and $\mathrm{d}\ln\langle A\rangle/\mathrm{d}\ln E_0$ as a function of $\ln E_0$ in three phase structures when the measurement frequency is 1 Hz are given. It is obvious that the differential curves of three phase structures show the same profile. The curve presents only slight changes at the beginning. Afterwards, $\mathrm{d}\ln\langle A\rangle/\mathrm{d}\ln E_0$ increases rapidly until reaches to a maximum then decreases drastically. At the end of the curve, $\mathrm{d}\ln\langle A\rangle/\mathrm{d}\ln E_0$ decreases slowly as the E_0 increases.

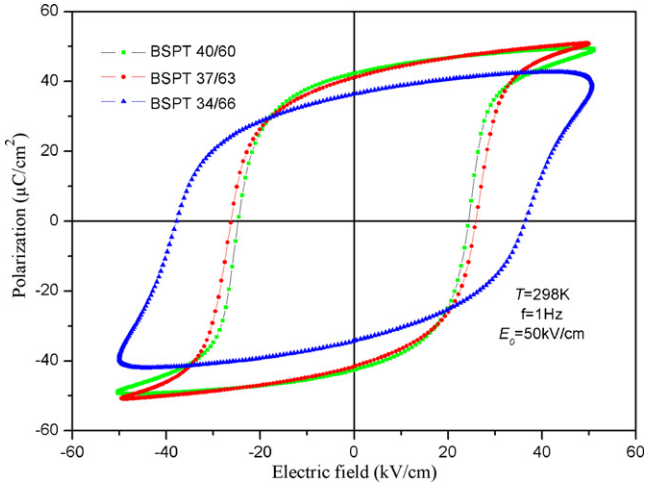

Fig. 3. Hysteresis loops for $(1-x)BiScO_3$–$xPbTiO_3$ ceramics with different phase structure (color online).

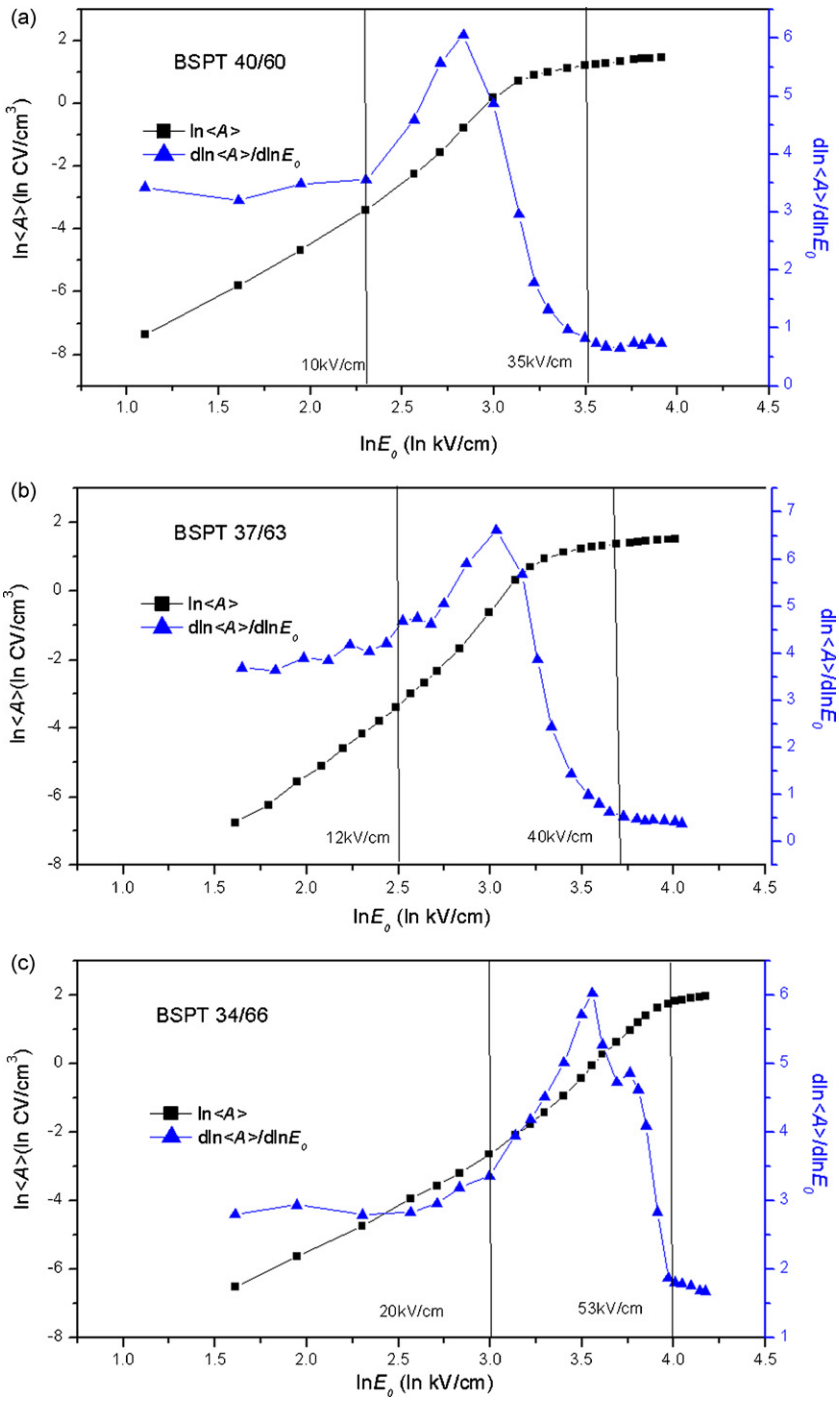

Fig. 4. The curves of $\ln\langle A\rangle$ and $\mathrm{d}\ln\langle A\rangle/\mathrm{d}\ln E_0$ as a function of $\ln E_0$ in three phase structures (a) BSPT40/60, (b) BSPT37/63, (c) BSPT34/66.

The curves between $\mathrm{d}\ln\langle A\rangle/\mathrm{d}\ln E_0$ and $\ln E_0$ show the same profile under all the measurement frequencies. From the changing tendency of differential curve, the curve can be divided into three parts with the increasing of E_0. The $\mathrm{d}\ln\langle A\rangle/\mathrm{d}\ln E_0$ in the first and third stage to some extent can be regarded as a constant. So in the first and third stage, there exist linear relations between $\ln\langle A\rangle$ and $\ln E_0$. But in the second stage, $\mathrm{d}\ln\langle A\rangle/\mathrm{d}\ln E_0$ varies dramatically, if there existed a linear relation in second stage, $\mathrm{d}\ln\langle A\rangle/\mathrm{d}\ln E_0$ in second stage should show only slight changes. Thus, $\ln\langle A\rangle$ and $\ln E_0$ can be fitted to $\ln\langle A\rangle = b + a\ln E_0$ in first and third stage.

As shown in Fig. 5, in the first stage, the slopes for the R phase, MPB and T phase are 3.28838 ± 0.09872 ($R^2 = 0.9973$), 3.88407 ± 0.08624 ($R^2 = 0.99656$) and 2.76381 ± 0.05636 ($R^2 = 0.99751$), respectively. And in the third stage, the slopes are 0.62136 ± 0.02067 ($R^2 = 0.98319$), 0.44964 ± 0.01397 ($R^2 = 0.99424$) and 0.72876 ± 0.03397 ($R^2 = 0.98309$). The same treatments have been done in a range of frequency from 0.1 to 100 Hz for each phase structure. The analogous linear behavior can be identified as the frequency increases and the three stage behaviors also exist in each frequency. All the slopes are within the fitting error. These three-stage behaviors between $\ln\langle A\rangle$

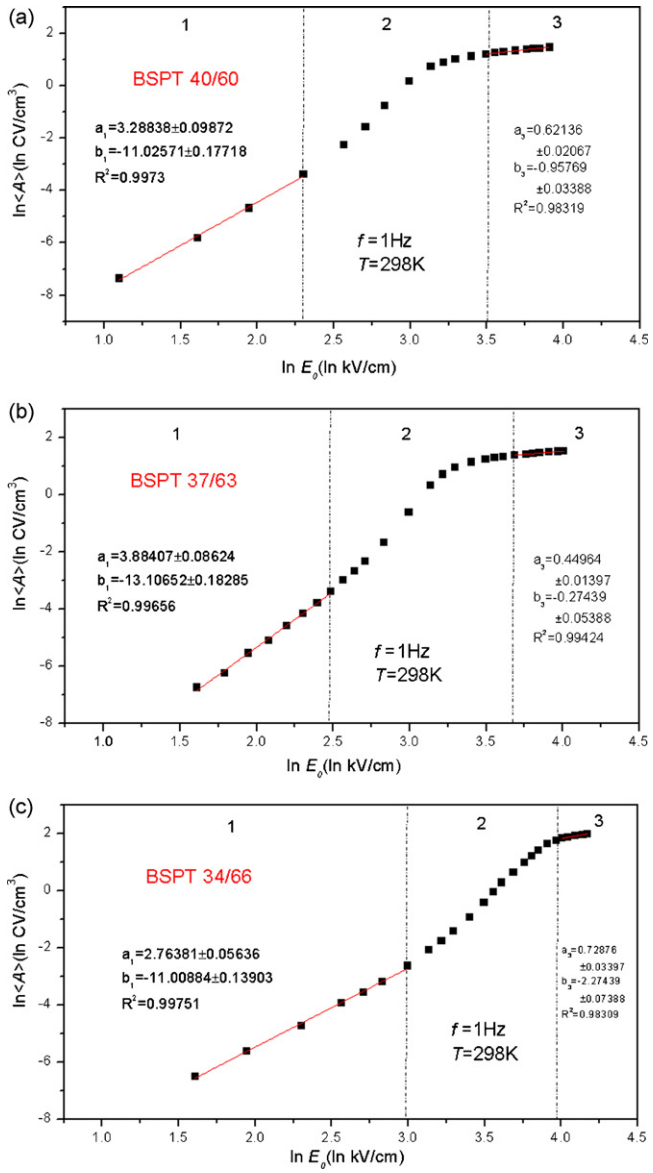

Fig. 5. The linear relations in BSPT ceramics between $\ln\langle A\rangle$ and $\ln E_0$ when f was 1 Hz in the first and third stage (a) BSPT40/60, (b) BSPT37/63, and (c) BSPT34/66.

and $\ln E_0$ are different from the existing two-stage behaviors [7,8].

In Fig. 6, we plot the normalized slope $a_i/a_{i-0.1\,\mathrm{Hz}}$ as a function of $\ln f$ in R phase structures as an example ($i = 1$–3, a_1 represents the slope in the first stage and $a_{1-0.1\,\mathrm{Hz}}$ represents the slope in the first stage when $f = 0.1$ Hz). It shows that a_1 is frequency-independent in the range of frequency from 0.1 to 100 Hz. In the first stage, a_1 to some extent can be regarded as the same in the whole frequency range. Similarly, the slopes of MPB and T phase in the first stage also show frequency-independent behavior and present slight changes in the whole frequency range. As for a_3, it is evident that a_3 increases with the increasing of f. In Fig. 5, the inset shows the exponential relationship exists between $a_3/a_{3-0.1\,\mathrm{Hz}}$ and $\ln f$ in BSPT40/60 with R phase structure,

$$\frac{a_3}{a_{3-0.1\ \mathrm{Hz}}} = 1.01017 + 0.02293\ \exp\left(\frac{\ln f}{1.26334}\right) \quad (1)$$

The relation between a_3 and f takes the form of

$$a_3 = 0.6081 + 0.014 f^{0.7916} \quad (2)$$

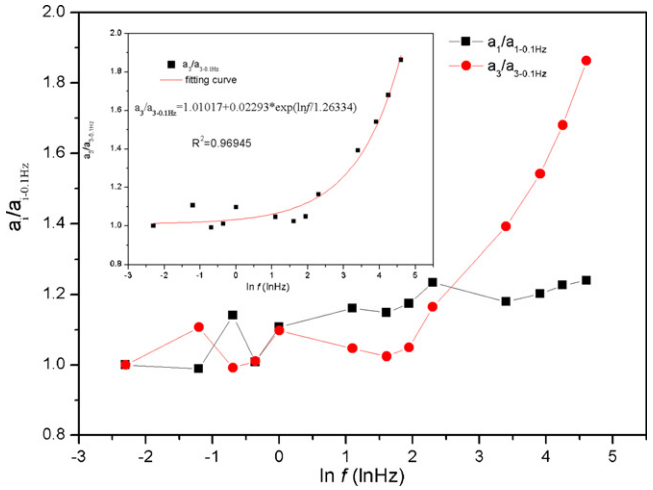

Fig. 6. The fitting curve between normalized slope a_3 and $\ln f$ in BSPT40/60 ceramics.

Similarly, the relations between a_3 and f in the BSPT37/63and BSPT34/66 are

$$a_3 = 0.45576 + 0.001 f^{1.2767} \quad (3)$$

and

$$a_3 = 0.7713 + 0.057 f^{1.1374} \quad (4)$$

It can be seen that the coefficient 0.7713 and 0.057 in Eq. (4) are larger than that in Eqs. (2) and (3), the effect of frequency on a_3 is more remarkable in the tetragonal structure.

From the above, the different behavior in each stage between $\ln\langle A\rangle$ and $\ln E_0$ strongly suggest different polarization behavior in each stage. In the first stage, the space charge polarization may be main polarization mechanism in this stage [15,16]. The space charge polarization can be attributed to accumulation and release of the mobile charge carriers that arise at the interface between two different interfaces [15–18]. Due to the low field, domain switch cannot be activated in this stage.

For the second stage, the polarization behavior can be regarded as domain switching mechanism [11,19–21]. The domain switch in this stage may be interpreted as a nucleation and growth process or a continuum domain process without nucleation and growth, which involves 180° domain and non-180° domain reorientation [19–21]. In the third stage, the slope in this region is much smaller than that in the first two stages. This can be explained as follows: as presented in Fig. 2, P_r in third stage to some extent can be regarded as a constant. This indicates that no more domains switch with the increasing of E_0. In other words, the amount of newly activated domains by the increasing of E_0 decreases dramatically in third stage. So the increment of energy dissipation with the increasing of E_0 in third stage decreases. In addition, the continuous realignment of the complex defects dipole perpendicularly to the electric field as the E_0 increases may reduce the energy barrier during the reverse process and lead to the decreasing of slope in third stage [21,22]. The increasing of slopes when frequency increases in third stage may be due to an increase of the dielectric losses at high frequencies.

In Fig. 5, it is obvious that the dividing points of two stages shift rightwards as the phase structure transforms from R phase to T phase. The first dividing points for rhombohedral, MPB and tetragonal phase are 10, 12 and 18 kV/cm respectively. And the second points are 35, 40 and 53 kV/cm respectively. Both of them shift to the larger side of the amplitude of field. Former studies showed that the internal stress for rhombohedral phase was smaller than that in tetragonal phase, and increased with increas-

ing c/a ratio in tetragonal compositions [23]. Furthermore, the amount of 90° domain increase as the phase structure evolves from rhombohedral phase to tetragonal phase [13], the presence of 90° domain inhibits the motion of 180° domain [24]. The study of dielectric and converse piezoelectric response showed that large lattice distortion in tetragonal samples produces a low mobility of ferroelectric–ferroelastic domain wall [25]. In Fig. 3, the E_c increases as the phase structure evolves from rhombohedral phase to tetragonal phase. This reflects the large lattice distortion in tetragonal samples and leads to a low mobility of ferroelectric–ferroelastic domain wall. Thus, these factors lead to a higher activate field of domain switch in the tetragonal phase and cause the shifting of dividing points.

4. Conclusions

In summary, the ferroelectric hysteresis loops of $(1-x)BiScO_3$–$xPbTiO_3$ ceramics with different phase structures were measured under different measurement conditions. The fitting results showed two linear relations existed between $\ln\langle A\rangle$ and $\ln E_0$ in the first and third field region. In the second region, no linear relation existed due to domain switching. These three-stage behaviors were distinct from the existing two-stage behaviors. The shifting of two dividing points as the phase structure varies from rhombohedral phase to tetragonal phase indicated in the tetragonal phase domain switching has a higher activation field.

Acknowledgements

This work was supported by National High Technology Research and Development Program (863 program) of China (Nos. 2007AA03Z106, 2006AA03Z431) and International Cooperation Program of SAST (No. 09520709200).

References

[1] R.E. Eitel, C.A. Randall, T.R. Shrout, S.E. Park, Jpn. J. Appl. Phys. 41 (2002) 2099–2104.
[2] S. Chen, X.L. Dong, C.L. Mao, F. Cao, J. Am. Ceram. Soc. 89 (2006) 3270–3272.
[3] H.X. Yan, H.T. Zhang, M.J. Reece, X.L. Dong, Appl. Phys. Lett. 87 (2005) 082911.
[4] J.F. Scott, Ferroelectric Memories, Springer, Berlin, 2000.
[5] J.M. Liu, H.P. Li, C.K. Ong, L.C. Lim, J. Appl. Phys. 86 (1999) 5198–5202.
[6] B. Pan, H. Yu, D. Wu, X.H. Zhou, J.M. Liu, Appl. Phys. Lett. 83 (2003) 1406–1408.
[7] R. Yimnirun, Y. Laosiritaworn, S. Wongsaenmai, S. Ananta, Appl. Phys. Lett. 89 (2006) 162901.
[8] R. Yimnirun, R. Wongmaneerung, S. Wongsaenmai, A. Ngamjarurojana, S. Ananta, Y. Laosiritaworn, Appl. Phys. Lett. 90 (2007) 112908.
[9] X.F. Chen, X.L. Dong, N.B. Feng, H.C. Nie, F. Cao, G.S. Wang, Y. Gu, H.L. He, Solid State Commun. 149 (2004) 663–666.
[10] N. Wongdamnern, A. Ngamjarurojana, Y. Laosiritaworn, S. Ananta, R. Yimnirun, J. Appl. Phys. 105 (2009) 044109.
[11] D. Viehland, J.F. Li, J. Appl. Phys. 90 (2001) 2995–3003.
[12] C. Jullian, J.F. Li, D. Viehland, Appl. Phys. Lett. 83 (2003) 1196–1198.
[13] C.A. Randall, R.E. Eitel, T.R. Shrout, D.I. Woodward, I.M. Reaney, J. Appl. Phys. 93 (2003) 9271–9274.
[14] R.E. Eitel, C.A. Randall, T.R. Shrout, S. Park, Jpn. J. Appl. Phys.: Part 1 41 (2002) 2099–2104.
[15] T.M. Kamel, F.X.N.M. Kools, G. De With, J. Eur. Ceram. Soc. 27 (2007) 2471–2479.
[16] T.H. Hölbling, N. Söylemezoğlu, R. Waser, J. Electroceram. 9 (2002) 87–100.
[17] M. Vollman, R. Waser, J. Am. Ceram. Soc. 77 (1994) 235–243.
[18] R. Waser, R. Hagenbeck, Acta Mater. 48 (2000) 797–825.
[19] D. Viehland, Y.H. Chen, J. Appl. Phys. 88 (2000) 6696–6707.
[20] S. Li, A.S. Bhalla, R.E. Newnham, L.E. Cross, C. Huang, J. Mater. Sci. 29 (1994) 1290–1294.
[21] M.H. Lente, J.A. Eiras, J. Appl. Phys. 89 (2001) 5093–5099.
[22] M.H. Lente, J.A. Eiras, J. Appl. Phys. 92 (2002) 2112–2117.
[23] Q.Y. Jiang, E.C. Subbarao, L.E. Cross, J. Appl. Phys. 75 (1994) 7433–7443.
[24] W. Li, M. Alexe, Appl. Phys. Lett. 91 (2007) 262903.
[25] J.E. Garcia, R. Perez, D.A. Ochoa, A. Albareda, M.H. Lente, J.A. Eiras, J. Appl. Phys. 103 (2008) 054108.